

# Efficient, high-performance pancreatic segmentation using multi-scale feature extraction

Moritz Knolle<sup>1,2,\*</sup>, Georgios Kaissis<sup>1,2,3,4\*</sup>, Friederike Jungmann<sup>1</sup>,  
Sebastian Ziegelmayer<sup>1</sup>, Daniel Sasse<sup>1</sup>, Marcus Makowski<sup>1</sup>, Daniel  
Rueckert<sup>2,4</sup>, and Rickmer Braren<sup>1,+</sup>

<sup>1</sup>Department of diagnostic and interventional Radiology, Technical  
University of Munich, Munich, Germany

<sup>2</sup>Institute for Artificial Intelligence and Data Science in Medicine and  
Healthcare, Technical University of Munich, Munich, Germany

<sup>3</sup>OpenMined Research

<sup>4</sup>Department of Computing, Imperial College London, London,  
United Kingdom

\* shared first authorship

+Corresponding author e-mail: rbraren@tum.de

## Abstract

### Rationale

For artificial intelligence-based image analysis methods to reach clinical applicability, the development of high-performance algorithms is crucial. For example, existent segmentation algorithms based on natural images are neither efficient in their parameter use nor optimized for medical imaging. Here we present *MoNet*, a highly optimized neural-network-based pancreatic segmentation algorithm focused on achieving high performance by efficient multi-scale image feature utilization.

### Methods

We developed *MoNet* a shallow, *U-Net*-like architecture based on repeated, dilated convolutions with decreasing dilation rates. The model was trained on publicly available pancreatic computed tomography (CT) scans in the portal-venous phase from the Medical Segmentation Decathlon (196 training and 85 validation scans) and tested for its out-of-sample generalization performance by evaluating the Dice coefficient on 85 manually segmented scans sourced from our institution’s picture archiving and communication system (PACS). We compared the model’s Dice coefficient and inference time against the standard architectures (*U-Net* and *Attention U-Net*).

### Results

*MoNet* achieved a mean $\pm$ STD Dice coefficient of  $0.70 \pm 0.1$  on the independent test data set (*U-Net*:  $0.50 \pm 0.2$ , *Attention U-Net*:  $0.37 \pm 0.6$ ) while utilizing 403,556 parameters (*U-Net*: 31,054,145, *Attention U-Net*: 31,753,349). Mean $\pm$ STD inference time was  $14.88 \pm 0.32s$  compared to  $45.34 \pm 1.77s$  for *U-Net* and  $53.30 \pm 0.53s$  for *Attention U-Net*.

### Conclusion

We present an optimized neural network architecture for pancreatic segmentation which provides performance competitive with the state-of-the-art on out-of-sample data while utilizing fewer parameters and requiring a fraction of inference time.

## Introduction

Pancreatic ductal adenocarcinoma (PDAC) is prognosticated to soon become the second leading cause of cancer-related death worldwide because of late diagnosis and diverse tumor biology [1]. Machine learning-based quantitative imaging workflows have demonstrated promising results in a variety of oncologic imaging workflows, such as the detection or sub-classification of lung [2] and breast [3] cancers in imaging data. Arguably, successes have been driven in part by the facility of automatic detection and segmentation of these tumor entities due to high-contrast to the surrounding tissue and high acquisition resolution of thoracic CT or mammography. To translate such applications to PDAC, e.g. to improve early diagnosis and non-invasive classification of known molecular tumor subtypes with differential outcome in response to available chemotherapy regimens, high-performance pancreatic segmentation algorithms will be instrumental. However, the success of automated segmentation algorithms in pancreatic CT imaging has hitherto been limited by the organ’s poor differentiability from adjacent structures of similar attenuation, variability in position and fat content and alterations due to pathology such as tumor or inflammation.

Existent work in deep learning-assisted pancreatic segmentation has focused on expanding previously available architectures such as the *U-Net*[4] into the three-dimensional context [5] or on improving segmentation results by incorporating attention mechanisms into the architecture[6]. These modifications however result in a further increase in the (already substantial) computational requirements and resulting costs of these architectures, rendering such *U-Net* derivatives impractical for cost-efficient utilization in rapid research workflows or in clinical practice. Here, we introduce *MoNet*, an optimized, shallow, *U-Net*-derived architecture achieving with state-of-the-art or higher performance in pancreatic segmentation, based on efficient multi-scale feature extraction using repeated decreasingly dilated convolution (RDDC) layers with two global down-sampling operations and a total of 403,556 parameters, a  $> 95\%$  parameter reduction compared to the original *U-Net* architecture.

## Methods

### Training, validation and independent testing datasets

All neural network architectures presented in this work were trained on the pancreas dataset from the Medical Segmentation Decathlon (MSD) [7]. A 70%/30% training-validation split was employed. Hence, 196 abdominal CT scans of the portal-venous contrast agent enhancement phase were used for training and 85 scans for validation. For processing, images were bilinearly down-sampled to  $256 \times 256$ , and the pancreas and tumor labels



Figure 1: Axial slice of a ground truth pancreas segmentation in an abdominal CT scan (MSD)

were merged yielding a two-class segmentation task. To assess out-of-sample performance, independent validation of the architectures was performed on an unseen, clinical PDAC dataset consisting of 85 abdominal CT scans in the portal-venous phase collected at our institution. All clinical data were collected according to Good Clinical Practice and in consent with the Declaration of Helsinki. The use of imaging data was approved by the institutional ethics committee and the requirement for informed written consent was waived. The pancreas including the tumor was manually segmented by a third-year radiology resident, then checked and corrected as necessary by a sub-specialized abdominal radiologist. An exemplary ground truth label mask superimposed on a CT slice from the training set is shown in Figure 1.

### Network architecture

The architecture of *MoNet* is depicted in Fig. 2. In brief, input tensors of shape  $B \times 256 \times 256 \times 1$ , with  $B$  denoting the batch size, are progressively down-sampled across the encoder branch of the network using convolutions with a stride length of 2, resulting in an  $X \times Y$  resolution of  $64 \times 64$  in the *bottleneck* segment of the network. The resulting feature maps are then progressively up-sampled by transposed convolution (*deconvolution*) in the decoder branch resulting in output masks of identical dimensions as the input. Each (de-)convolution block consists of a  $3 \times 3$  convolutional layer followed by batch normalization and an *exponential linear unit* (ELU) activation. At every stage in the *U-Net*-like architecture, the convolution blocks are followed by a *repeated decreasingly dilated convolution* (RDDC) block (Fig. 3), consisting of four successive convolutional blocks as described above, but employing dilated convolutions [8] with a decreasing dilation rate (4, 3, 2, 1, respectively). A feature extraction strategy that has been shown to perform well for small objects[9]. Each convolutional block within a *RDDC* block is

followed by a spatial dropout layer[10]. Finally, residual-type longitudinal (short) connections are employed within each RDDC block and transverse (long) skip connections are employed between the encoder and the decoder branch to assist signal and gradient flow as originally described in [4, 11].

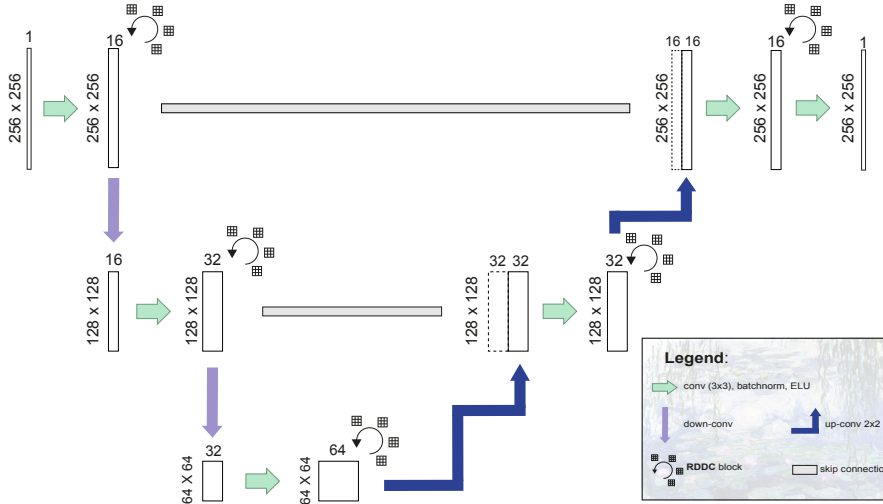


Figure 2: Schematic representation of the *MoNet* architecture.

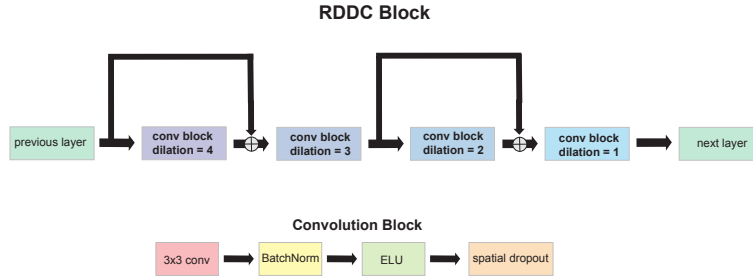


Figure 3: Schematic representation diagram of a RDDC block (top) and the constituent convolutional blocks (bottom).

## Model training

All architectures were trained to convergence using the *Nesterov-Adam optimizer*[12] with an initial learning rate of  $5 \times 10^{-4}$  and learning rate decay by a factor 10 upon validation loss stagnation for  $\geq 2$  epochs. Weights were initialized using uniform He-initialization and the Dice loss was used to train all networks. Data augmentation was used in the form of random rotations up to  $10^\circ$ , random zoom ( $\pm 0.25$ ) and random pixel shifts of a maximum

magnitude of 0.2 of the image height/width. Data augmentation was validated and chosen based on advice from a senior radiologist to represent plausible data expected to be encountered in real-world clinical use settings when imaging the pancreas.

## Performance Assessment

We compared *MoNet*'s out-of-sample generalisation performance to the following two *U-Net* [4] variants:

- original *U-Net*, 64 base filters (*U-Net*)
- Attention-gated *U-Net*, 2D, 64 base filters (*Attention U-Net*)

For all performance comparisons, repeated testing was performed under identical circumstances (no concurrent network traffic, all non-essential operating system processes suspended, identical CPU power settings). Mean inference times and Dice scores were compared using the Student's t-test with multiple testing correction.

## Results

### Inference-time comparison

A comparison of the time required for performing inference with 150  $256 \times 256$  images on CPU (2.4GHz 8-Core Intel Core i9) was performed with identical batch size and otherwise consistent environment for *U-Net*, *Attention U-Net* (2D) and *MoNet*. *MoNet* significantly outperformed both *U-Net* and *Attention U-Net* with regards to inference time (Student's t-test with multiple testing correction  $p < 0.0001$  in all cases, Table 1).

Architecture	Mean $\pm$ STD inference times (sec), N=5 repetitions
<i>U-Net</i>	$45.34 \pm 1.77$
<i>Attention U-Net</i>	$53.30 \pm 0.53$
<i>MoNet (ours)</i>	<b><math>14.88 \pm 0.32</math></b>

Table 1: Inference time for a CT scan of 150 slices at  $256 \times 256$  resolution, results averaged over 5 runs under identical setup.

### Segmentation Performance Comparison

*MoNet* performed on par with other *U-Net* variants on the validation dataset (all Student's t-test after multiple testing correction *non-significant*) while outperforming the other *U-Net* variants on the independent validation dataset (all Student's t-test after multiple testing correction  $p < 0.0001$ ). Results are summarized in Table 2.

Architecture	Parameter count	Mean±STD Dice, MSD	Mean±STD Dice, IVD
<i>MoNet (ours)</i>	403,556	<b>0.74 ± 0.11</b>	<b>0.70 ± 0.1</b>
<i>U-Net</i>	31,054,145	0.70 ± 0.15	0.50 ± 0.2
<i>Attention U-Net</i>	31,753,349	0.66 ± 0.15	0.37 ± 0.6

Table 2: Comparison of *MoNet* with other *U-Net* variants tested on the MSD and the independent validation set (IVD) (both N=85 scans).

## Discussion

We here present an efficient, high-performance *U-Net*-like segmentation algorithm for pancreatic segmentation and show significant inference speed gains on CPU hardware while maintaining or exceeding the segmentation performance of similar algorithms. The poor prognosis and increasing incidence of PDAC [13, 1] mandate the development of enhanced diagnosis and treatment strategies. Our recent findings suggest that quantitative image analysis can identify molecular subtypes related to different response to chemotherapeutic drugs [14] or predict patient survival [15]. Automated region-of-interest definition increases the reliability and validity of such findings, and offers substantial time savings compared to manual expert-based segmentation. However, the widespread application of automatic segmentation algorithms will depend both, on their real-world segmentation performance and on ease of deployment on a wide range of hardware environments, e.g. on hardware lacking graphics processing units.

The work presented provides state-of-the-art segmentation performance with substantial efficiency gains through the utilization of higher resolution feature maps in the *bottleneck* section of the network, making it suitable both for rapid prototyping and for large-scale deployment of e.g. decentralized machine learning workflows [16]. Network architectures with few parameters are therefore an excellent strategy to reduce network traffic.

*MoNet* was trained to segment the entire pancreas including the tumor. This approach is owing to the fact that the exact delineation of the tumor border is often times infeasible and supported by literature findings noting the importance of the peritumoral tissue in PDAC [17, 18, 19] and in other tumor entities [20].

Recent work on semantic segmentation provides evidence in favor of architectures performing image feature extraction at multiple scales by utilizing dilated convolutions instead of relying merely on the scale-decreasing backbones employed in traditional fully convolutional architectures [21, 22, 9, 23]. Our work corroborates this notion, since multi-scale feature extraction combined with larger receptive fields at the same hierarchical level seem to capture both more robust and higher quality features compared to the fixed kernel size design encountered in *U-Net*-like architectures. Moreover, architectures with several down-sampling operations and/or many filters

such as the 64-filter *U-Net* (with 4 down-sampling stages) cannot leverage the large number of parameters sufficiently well to warrant their utilization at least in medical imaging tasks, typically characterized by a lack of large datasets and by small segmentation targets (such as the pancreas).

Furthermore, segmentation algorithms are often trained on publicly available and/or single-institutional data such as the pancreas dataset from MSD, which has recently been identified to potentially create generalization challenges to data collected at different centers[24]. Our results show that *MoNet* using repeated decreasingly dilated convolutions extracts more robust features that generalize better to out-of-sample data than current methods, as shown by *MoNet*'s performance on the independent validation set.

Our work is not without limitations. The generalizability of our findings is still limited due to the single-institution independent validation set and the relatively small sample size. All tested algorithms would have benefited from larger training sets and from performance evaluation on additional multi-center data sets. Furthermore, we only compared our algorithm against algorithms based on the use of a single 2D-*U-Net*-style network. Algorithms such as *nnU-Net* [25] based on *U-Net* ensembles offer superior performance, however at the expense of high computational and post-processing requirements and thus much slower inference times (especially on CPU).

## Conclusion

In conclusion, we propose an efficient, state-of-the-art performance pancreatic segmentation algorithm which can benefit both, radiological research and clinical translation of artificial intelligence workflows in medical imaging by providing consistent, high-quality segmentation for both *radiomics* and machine learning tasks.

## Source code and data availability

Source code for *MoNet* based on TensorFlow is available at <https://github.com/TUM-AIMED/MoNet>. The training datasets are available from <http://medicaldecathlon.com/>. The independent test set data contains confidential patient information and cannot be shared publicly.

## References

- [1] E. A. Collisson, P. Bailey, D. K. Chang, and A. V. Biankin, "Molecular subtypes of pancreatic cancer," *Nature Reviews Gastroenterology & Hepatology*, vol. 16, no. 4, pp. 207–220, 2019.



- [2] D. Ardila, A. P. Kiraly, S. Bharadwaj, B. Choi, J. J. Reicher, L. Peng, D. Tse, M. Etemadi, W. Ye, G. Corrado, D. P. Naidich, and S. Shetty, “End-to-end lung cancer screening with three-dimensional deep learning on low-dose chest computed tomography,” *Nature Medicine*, vol. 25, pp. 954–961, may 2019.
- [3] S. M. McKinney, M. Sieniek, V. Godbole, J. Godwin, N. Antropova, H. Ashrafiyan, T. Back, M. Chesus, G. C. Corrado, A. Darzi, *et al.*, “International evaluation of an ai system for breast cancer screening,” *Nature*, vol. 577, no. 7788, pp. 89–94, 2020.
- [4] O. Ronneberger, P. Fischer, and T. Brox, “U-net: Convolutional networks for biomedical image segmentation,” in *International Conference on Medical image computing and computer-assisted intervention*, pp. 234–241, Springer, 2015.
- [5] F. Milletari, N. Navab, and S.-A. Ahmadi, “V-net: Fully convolutional neural networks for volumetric medical image segmentation,” in *2016 fourth international conference on 3D vision (3DV)*, pp. 565–571, IEEE, 2016.
- [6] O. Oktay, J. Schlemper, L. L. Folgoc, M. Lee, M. Heinrich, K. Misawa, K. Mori, S. McDonagh, N. Y. Hammerla, B. Kainz, *et al.*, “Attention u-net: Learning where to look for the pancreas,” *arXiv preprint arXiv:1804.03999*, 2018.
- [7] A. L. Simpson, M. Antonelli, S. Bakas, M. Bilello, K. Farahani, B. Van Ginneken, A. Kopp-Schneider, B. A. Landman, G. Litjens, B. Menze, *et al.*, “A large annotated medical image dataset for the development and evaluation of segmentation algorithms,” *arXiv preprint arXiv:1902.09063*, 2019.
- [8] M. Holschneider, R. Kronland-Martinet, J. Morlet, and P. Tchamitchian, “A real-time algorithm for signal analysis with the help of the wavelet transform,” in *Wavelets*, pp. 286–297, Springer, 1990.
- [9] R. Hamaguchi, A. Fujita, K. Nemoto, T. Imaizumi, and S. Hikosaka, “Effective use of dilated convolutions for segmenting small object instances in remote sensing imagery,” in *2018 IEEE winter conference on applications of computer vision (WACV)*, pp. 1442–1450, IEEE, 2018.
- [10] J. Tompson, R. Goroshin, A. Jain, Y. LeCun, and C. Bregler, “Efficient object localization using convolutional networks,” in *Proceedings of the IEEE conference on computer vision and pattern recognition*, pp. 648–656, 2015.

- [11] K. He, X. Zhang, S. Ren, and J. Sun, “Deep residual learning for image recognition,” in *Proceedings of the IEEE conference on computer vision and pattern recognition*, pp. 770–778, 2016.
- [12] T. Dozat, “Incorporating nesterov momentum into adam,” 2016.
- [13] American Cancer Society, “Cancer Facts & Figures 2020.”
- [14] G. A. Kaissis, S. Ziegelmayer, F. K. Lohöfer, F. N. Harder, F. Jungmann, D. Sasse, A. Muckenhuber, H.-Y. Yen, K. Steiger, J. Siveke, H. Friess, R. Schmid, W. Weichert, M. R. Makowski, and R. F. Braren, “Image-Based Molecular Phenotyping of Pancreatic Ductal Adenocarcinoma,” *Journal of Clinical Medicine*, vol. 9, p. 724, mar 2020.
- [15] G. A. Kaissis, F. Jungmann, S. Ziegelmayer, F. K. Lohöfer, F. N. Harder, A. M. Schlitter, A. Muckenhuber, K. Steiger, R. Schirren, H. Friess, R. Schmid, W. Weichert, M. R. Makowski, and R. F. Braren, “Multiparametric Modelling of Survival in Pancreatic Ductal Adenocarcinoma Using Clinical, Histomorphological, Genetic and Image-Derived Parameters,” *Journal of Clinical Medicine*, vol. 9, p. 1250, apr 2020.
- [16] W. Li, F. Milletari, D. Xu, N. Rieke, J. Hancox, W. Zhu, M. Baust, Y. Cheng, S. Ourselin, M. J. Cardoso, and A. Feng, “Privacy-Preserving Federated Brain Tumour Segmentation,” in *Machine Learning in Medical Imaging*, pp. 133–141, Springer International Publishing, 2019.
- [17] A. S. Bauer, P. V. Nazarov, N. A. Giese, S. Beghelli, A. Heller, W. Greenhalf, E. Costello, A. Muller, M. Bier, O. Strobel, T. Hackert, L. Vallar, A. Scarpa, M. W. Büchler, J. P. Neoptolemos, S. Kreis, and J. D. Hoheisel, “Transcriptional variations in the wider peritumoral tissue environment of pancreatic cancer,” *International Journal of Cancer*, vol. 142, pp. 1010–1021, oct 2017.
- [18] N. Fukushima, J. Koopmann, N. Sato, N. Prasad, R. Carvalho, S. D. Leach, R. H. Hruban, and M. Goggins, “Gene expression alterations in the non-neoplastic parenchyma adjacent to infiltrating pancreatic ductal adenocarcinoma,” *Modern Pathology*, vol. 18, pp. 779–787, mar 2005.
- [19] J. R. Infante, H. Matsubayashi, N. Sato, J. Tonascia, A. P. Klein, T. A. Riall, C. Yeo, C. Iacobuzio-Donahue, and M. Goggins, “Peritumoral Fibroblast SPARC Expression and Patient Outcome With Resectable Pancreatic Adenocarcinoma,” *Journal of Clinical Oncology*, vol. 25, pp. 319–325, jan 2007.
- [20] Q. Sun, X. Lin, Y. Zhao, L. Li, K. Yan, D. Liang, D. Sun, and Z.-C. Li, “Deep learning vs. radiomics for predicting axillary lymph node

metastasis of breast cancer using ultrasound images: Don't forget the peritumoral region," *Frontiers in Oncology*, vol. 10, jan 2020.

- [21] X. Du, T.-Y. Lin, P. Jin, G. Ghiasi, M. Tan, Y. Cui, Q. V. Le, and X. Song, "Spinenet: Learning scale-permuted backbone for recognition and localization," in *Proceedings of the IEEE/CVF Conference on Computer Vision and Pattern Recognition*, pp. 11592–11601, 2020.
- [22] L.-C. Chen, G. Papandreou, F. Schroff, and H. Adam, "Rethinking atrous convolution for semantic image segmentation," *arXiv preprint arXiv:1706.05587*, 2017.
- [23] F. Yu and V. Koltun, "Multi-scale context aggregation by dilated convolutions," *arXiv preprint arXiv:1511.07122*, 2015.
- [24] L. Zhang, X. Wang, D. Yang, T. Sanford, S. Harmon, B. Turkbey, B. J. Wood, H. Roth, A. Myronenko, D. Xu, *et al.*, "Generalizing deep learning for medical image segmentation to unseen domains via deep stacked transformation," *IEEE Transactions on Medical Imaging*, 2020.
- [25] F. Isensee, J. Petersen, A. Klein, D. Zimmerer, P. F. Jaeger, S. Kohl, J. Wasserthal, G. Koehler, T. Norajitra, S. Wirkert, *et al.*, "nnu-net: Self-adapting framework for u-net-based medical image segmentation," *arXiv preprint arXiv:1809.10486*, 2018.